Intraband absorption in InAs/GaAs quantum dot infrared photodetectors - effective mass vs. $k \cdot p$ modelling

N Vukmirović[1], Ž Gačević[2]‡, Z Ikonić[1], D Indjin[1], P Harrison[1] and V Milanović[2]

[1]School of Electronic and Electrical Engineering, University of Leeds, Leeds LS2 9JT, UK

[2]Faculty of Electrical Engineering, University of Belgrade, Bulevar kralja Aleksandra 73, 11120 Belgrade, Serbia

E-mail: `eennv@leeds.ac.uk`

Abstract. Theoretical modelling of the intraband absorption spectrum in InAs/GaAs quantum dot infrared photodetectors is performed for several typical structures reported in the literature. The calculations are performed within the framework of the two methods: a simple and so far widely used effective mass method with the values of conduction band offset and the effective mass modified to take account of the effects of strain and band mixing on average and the more realistic 8-band $k \cdot p$ method with the strain distribution taken into account via the continuum mechanical model. Both methods give qualitatively the same results, however the peak positions obtained within the effective mass approach are blue shifted and the absorption cross-sections overestimated, compared to the more accurate $k \cdot p$ approach.

‡ Present address: Instituto de Energía Solar, Avenida Complutense s/n, 28040 Madrid, España

1. Introduction

Quantum dot infrared photodetectors (QDIPs) comprising III-As self assembled quantum dots have become a very important technology for the detection of mid- and far infrared electromagnetic radiation [1–15]. Since their initial realization and demonstration [1–3], there has been a lot of experimental success leading to permanent improvements in their performance. For example, the concept of a current blocking layer [4, 5] was introduced to reduce dark current. Quantum dots-in-a-well photodetectors [6–8] provide a way to tune the detection wavelength within a certain range by changing the well width and focal plane arrays based on QDIPs have also been demonstrated [9, 10]. Most recently, room temperature operation of a resonant tunneling QDIP has been achieved [11].

Following the experimental success in the field, there have been several theoretical studies of intraband absorption in QDIPs aimed to understand the detection process and assign the experimental peaks to transitions between certain states. In these studies, the energy levels and wave functions in quantum dots, and then the absorption spectra, have been calculated using mostly the 1-band effective mass approach [16–20], but also the 8-band $k \cdot p$ method [21]. In InAs/GaAs, the most commonly used material system, the large lattice mismatch induces a strong strain field and the small energy gap of InAs causes significant band-mixing; effects that the 1-band method can hardly take into account. The 8-band $k \cdot p$ method is therefore obviously a more realistic model, however the simpler and faster effective mass method is almost exclusively used [16–20], and the question arises whether it may still perform well enough to be useful for modelling the intraband absorption spectrum. One of the aims of this work is therefore to compare the calculated theoretical spectra for several experimentally realized QDIPs, obtained by the two methods and quantify the differences in the results. This contribution will allow one to have a quantitative measure of the inherent limitations of the effective mass method. Another aim is to simulate several typical QDIP structures reported in the literature and compare the results obtained by the 8-band $k \cdot p$ method with the experimental results.

2. Theoretical models

In this section, we shall review the two theoretical models used so far to model QDIP absorption spectra and describe the method used in this work to solve them. It is assumed throughout this paper that the quantum dot shape has cylindrical symmetry. In most of the QDIPs reported in literature, the dots have the shape of lens [17], cone [22] or truncated cone [7, 23], all belonging to the class of cylindrically symmetric dots.

2.1. Effective mass model

Within the framework of the effective mass method the Hamiltonian is given by

$$\hat{H} = -\boldsymbol{k}\frac{\hbar^2}{2m^*(\boldsymbol{r})}\boldsymbol{k} + V(\boldsymbol{r}) + |e|Fz, \tag{1}$$

where k_i ($i \in \{1, 2, 3\}$) is the differential operator $k_i = -i\frac{\partial}{\partial x_i}$, $\boldsymbol{F} = F\boldsymbol{e}_z$ is the electric field oriented along the $z-$direction, $m^*(\boldsymbol{r})$ is the position-dependent effective mass and $V(\boldsymbol{r})$ the position-dependent potential, both assumed constant within the dot and within the matrix (and within the well in the case of quantum dots-in-a-well structure). The modified values of the effective mass in the dot of $m^* = 0.04\,m_0$ [24] (where m_0 is the free electron mass) and the conduction band offset $V_0 = 450\,\mathrm{meV}$ [25] are used to take the averaged effect of strain into account. The same recipe as in [26] for the order of differential and multiplication operators was used throughout this work.

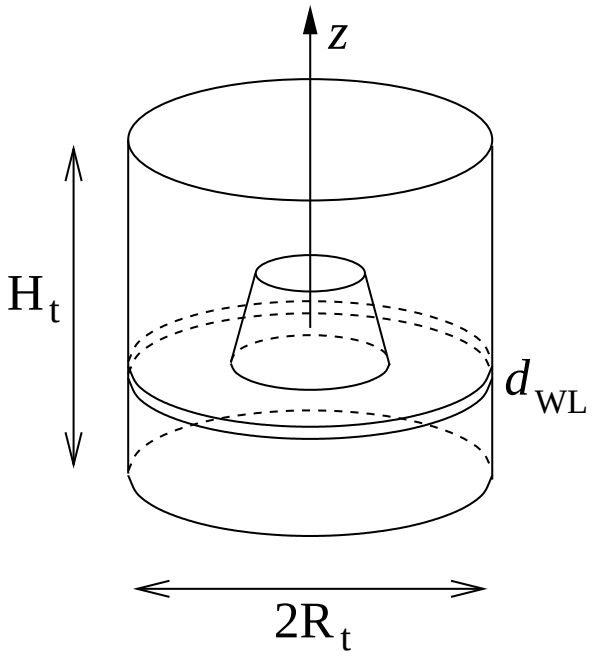

Figure 1. Schematic view of a quantum dot in an embedding cylinder of radius R_t and height H_t. The wetting layer width is d_{WL}.

The orthonormal wave function expansion method was used to find the eigenenergies and the corresponding wave functions. The method is based on embedding the dot in a cylinder of radius R_t and height H_t (see figure 1) and assuming the wave function as a linear combination of the expansion basis functions

$$\psi(\boldsymbol{r}) = \sum_{nl} A_{nl} b_{nml}(r, z, \varphi), \tag{2}$$

with the coefficients A_{nl} ($n \in \{1, \ldots, n_{max}\}$ and $l \in \{-l_{max}, \ldots, l_{max}\}$) to be determined. The basis functions b_{nml} are given by

$$b_{nml}(r, z, \varphi) = f_{nm}(r) g_l(z) \Phi_m(\varphi), \tag{3}$$

where

$$\begin{aligned} f_{nm}(r) &= \frac{\sqrt{2}}{R_t} \frac{J_m(k_{nm} r)}{\left| J_{|m|+1}(k_{nm} R_t) \right|}, \\ g_l(z) &= \frac{1}{\sqrt{H_t}} e^{i \frac{2\pi}{H_t} l z}, \\ \Phi_m(\varphi) &= \frac{1}{\sqrt{2\pi}} e^{i m \varphi}, \end{aligned} \tag{4}$$

where l and m are integers and n is a positive integer. J_m is a Bessel function of order m and $k_{nm} R_t$ is its n-th zero. Due to the cylindrical symmetry of the dots, the Hamiltonian commutes with the $z-$component of the orbital angular momentum, whose eigenvalue m is then a good quantum number and therefore in (2) the summation needs to be performed over n and l only.

After substituting the expansion (2) into the Hamiltonian eigenvalue problem one arrives at an eigenvalue problem of the Hamiltonian matrix

$$\sum_{n'l'} H_{nml,n'ml'} A_{n'l'} = E A_{nl}, \tag{5}$$

where

$$H_{nml,n'm'l'} = \int_V b^*_{nml} \hat{H} b_{n'm'l'} \, r \, \mathrm{d}r \, \mathrm{d}z \, \mathrm{d}\varphi \tag{6}$$

and the integration is performed over the volume of the embedding cylinder. The one-band Hamiltonian contains only the terms of the forms T_1, T_2 and T_3 (see Appendix) and their corresponding Hamiltonian matrix elements can be evaluated as shown in the Appendix.

The Hamiltonian $\hat{H}'$ of the interaction with the electromagnetic field is obtained by replacing $\boldsymbol{k}$ with $\boldsymbol{k} + \frac{e}{\hbar}\boldsymbol{A}$ in the Hamiltonian [27] (where $\boldsymbol{A} = A\,\boldsymbol{\varepsilon}$ is the magnetic vector potential, $\boldsymbol{\varepsilon}$ is the polarization vector of the radiation, e the magnitude of the elementary charge and $\hbar$ the reduced Planck's constant), i.e. $\hat{H}' = \hat{H}(\boldsymbol{k} + \frac{e}{\hbar}\boldsymbol{A}) - \hat{H}(\boldsymbol{k})$. In the dipole approximation $\boldsymbol{A}$ is considered constant in space, and furthermore all the terms quadratic in $\boldsymbol{A}$ are neglected. The optical cross section of the $i \to f$ transition due to absorption of electromagnetic radiation of angular frequency ω is given by [28]

$$\sigma^{\boldsymbol{\varepsilon}}_{if}(\omega) = \frac{2\pi}{\overline{n}\varepsilon_0 c \omega} \left| \mathcal{M}^{\boldsymbol{\varepsilon}}_{if} \right|^2 g(E_f - E_i - \hbar\omega, 2\sigma), \tag{7}$$

where $\overline{n}$ is the refraction index, c the speed of light in vacuum, ε_0 the vacuum dielectric constant and E_f and E_i are the energies of the final and the initial state, respectively. $\mathcal{M}^{\boldsymbol{\varepsilon}}_{if} = \left\langle i \left| \hat{H}' \right| f \right\rangle / A$ is the matrix element which depends only on the direction $\boldsymbol{\varepsilon}$ of light polarization and not on the amplitude of A. The inhomogeneous broadening due to size

inhomogeneity of the quantum dot ensemble was taken into account by replacing the delta function in Fermi's golden rule with a Gaussian given by

$$g(x, 2\sigma) = \frac{1}{\sigma\sqrt{2\pi}} \exp\left(-\frac{x^2}{2\sigma^2}\right). \tag{8}$$

The matrix element is equal to

$$\mathcal{M}_{if}^{\boldsymbol{\epsilon}} = \sum_{nl} \sum_{n'l'} A_{nl}^{i*} A_{n'l'}^{f} G(nl, n'l'), \tag{9}$$

where the superscripts i and f refer to the initial and final state and the perturbation Hamiltonian matrix elements

$$G(nl, n'l') = \frac{1}{A} \int_V b_{nml}^* \hat{H}' b_{n'ml'} \, r \, \mathrm{d}r \, \mathrm{d}z \, \mathrm{d}\varphi \tag{10}$$

are of the form T_5 (see Appendix) and can be therefore calculated in a similar manner. From the last two expressions, the selection rules can easily be established: $\Delta m = 0$ for absorption of $z-$polarized radiation and $|\Delta m| = 1$ for in-plane polarized radiation.

2.2. 8-band $k \cdot p$ model

Within the framework of the 8-band $k \cdot p$ method the state of the system is a sum of slowly varying envelope functions $\psi_i(\boldsymbol{r})$ multiplied by the bulk Bloch functions $|i\rangle$

$$|\Psi\rangle = \sum_{i=1}^{8} \psi_i(\boldsymbol{r}) |i\rangle, \tag{11}$$

and the Hamiltonian is equal to $\hat{H} = \hat{H}_k + \hat{H}_s + |e|Fz$, where $\hat{H}_k$ is the kinetic part and $\hat{H}_s$ the strain part of the Hamiltonian whose explicit forms are given in [29]. The envelope functions then satisfy the following system of coupled partial differential equations:

$$\sum_{j=1}^{8} \hat{H}_{ij} \psi_j(\boldsymbol{r}) = E \psi_i(\boldsymbol{r}). \tag{12}$$

The symmetry of the kinetic part of the 8-band $k \cdot p$ Hamiltonian $\hat{H}_k$ applied to cylindrically symmetric quantum dots is equal to the intersection of the symmetry of the geometrical shape of the dot and the symmetry of the zinc-blende crystal lattice. Since the crystal symmetry is lower than cylindrical it turns out that the system considered is only C_4 symmetric. However, the deviations of the Hamiltonian from the cylindrically symmetric form are only slight and one often employs the axial approximation [30] in which $\hat{H}_k$ becomes exactly axially symmetric. This is highly desirable as such an approximation effectively reduces the problem from a three dimensional to a two dimensional and therefore significantly reduces the computational cost, without influencing the accuracy. Such an approximation is therefore used in this work, too. Furthermore, the strain part $\hat{H}_s$ also slightly deviates from the cylindrically symmetric form and it would also have to be modified to be able to exploit the cylindrical symmetry and reduce the computational complexity. A slightly different approach is used here. The wave functions are assumed in the form they would have if the

Hamiltonian was exactly cylindrically symmetric, and therefore its parts that deviate from symmetry give a zero contribution in the Hamiltonian matrix elements (15).

Since the 8-band model inherently takes into account the spin-orbit interaction, the good quantum number in this case is the quantum number m_f (where m_f is half integer) of the $z-$component of the total orbital angular momentum [30] (rather than just the orbital angular momentum) given as a sum of the orbital angular momentum of the envelope function and total angular momentum of the Bloch function. The envelope functions of the quantum state having m_f can then be assumed in the form

$$\psi_i(\boldsymbol{r}) = \sum_{nl} A_{inl} b_{nm(i)l}(r, z, \varphi), \tag{13}$$

where $m(i) = m_f - m_j(i)$ and $m_j(i)$ is the eigenvalue of the z-component of the total angular momentum of the Bloch function $|i\rangle$ (its explicit values for one choice of the Bloch function basis can be found for example in [26]). After inserting the envelope function expansion of (13) into the Hamiltonian eigenvalue problem (12) one arrives at

$$\sum_{i'n'l'} H_{inm(i)l,i'n'm(i')l'} A_{i'n'l'} = E A_{inl}, \tag{14}$$

where

$$H_{inml,i'n'm'l'} = \int_V b^*_{nml} \hat{H}_{ii'} b_{n'm'l'}\, r\, \mathrm{d}r\, \mathrm{d}z\, \mathrm{d}\varphi. \tag{15}$$

The 8-band Hamiltonian contains the terms of the form $T_1 - T_{10}$ (see Appendix), whose corresponding Hamiltonian matrix elements are given in the Appendix.

The strain was modelled using the continuum mechanical model and the strain distribution was found using the finite element method in a manner that follows. The total elastic strain energy in the continuum mechanical model is given by [31]

$$W = \frac{1}{2} \int \mathrm{d}V \sum_{ijkl} \lambda_{ijkl} \left[e_{ij}(\boldsymbol{r}) - e^{(0)}_{ij}(\boldsymbol{r}) \right] \left[e_{kl}(\boldsymbol{r}) - e^{(0)}_{kl}(\boldsymbol{r}) \right], \tag{16}$$

where $e_{ij}(\boldsymbol{r})$ are the elastic strain tensor components, λ_{ijkl} is the elastic modulus tensor and $e^{(0)}_{ij}(\boldsymbol{r})$ the local intrinsic strain induced by the changes in the lattice constant

$$e^{(0)}_{ij}(\boldsymbol{r}) = \frac{a(\boldsymbol{r}) - a}{a}, \tag{17}$$

where $a(\boldsymbol{r})$ is the unstrained lattice constant at $\boldsymbol{r}$ and a the GaAs substrate lattice constant. In the crystals with zinc-blende crystal lattice the elastic tensor is of the form

$$\lambda_{ijkl} = C_{12}\delta_{ij}\delta_{kl} + C_{44}\left(\delta_{ik}\delta_{jl} + \delta_{il}\delta_{jk}\right) + C_{an} \sum_{p=1}^{3} \delta_{ip}\delta_{jp}\delta_{kp}\delta_{lp}, \tag{18}$$

where C_{12}, C_{44} and $C_{an} = C_{11} - C_{12} - 2C_{44}$ are the elastic constants. In order to find the strain distribution, the continuum space is discretized on a nonuniform rectangular grid and the components of the displacement in each point of space are expressed in terms of the displacements in the 8 neighbouring nodes of the grid, where first order Lagrange interpolation is used. Consequently, the elastic energy of the system W is a quadratic functional of the displacements at the nodes of the grid. Its minimization

therefore leads to a sparse system of linear equations for the displacements at the nodes, which is solved using the conjugate gradient method [32].

Within the framework of the $k \cdot p$ method the perturbation Hamiltonian is obtained by performing the same replacement in the kinetic part of the Hamiltonian as in the case of effective mass method. The absorption matrix element is then given by

$$\mathcal{M}_{if}^{\boldsymbol{\varepsilon}} = \sum_{inl} \sum_{i'n'l'} A_{inl}^{i*} A_{i'n'l'}^{f} G(inl, i'n'l'), \tag{19}$$

where the superscripts i and f refer to the initial and final state and the perturbation Hamiltonian matrix elements

$$G(inl, i'n'l') = \frac{1}{A} \int_V \mathrm{d}^3\boldsymbol{r} b_{nm(i)l}^{*} \hat{H}' b_{n'm(i')l'} \tag{20}$$

are of one of the forms T_1, T_4 and T_5 (see Appendix) and can be therefore calculated in a similar manner. After explicit calculation one can straightforwardly derive the selection rules: $\Delta m_f = 0$ for $z-$polarized radiation and $|\Delta m_f| = 1$ for in-plane polarized radiation.

3. Results

The two methods described in section 2 have been applied to calculate the optical absorption matrix elements and the intraband absorption spectra for quantum dots of several different shapes and sizes reported for experimentally realized QDIPs. In typical QDIP operating conditions only the ground state is significantly occupied as the occupation of the excited states would lead to a much larger dark current. The intraband absorption spectrum is therefore calculated by adding the contributions from transitions from the ground state to each of the excited states (bound or continuum). The material parameters in the calculation were taken from [33]. The standard deviation of the Gaussian lineshape was taken to be equal to 10% of the transition energy in the case of the transitions to bound states and 20% in the case of the transitions to continuum states. These are the typical values observed in the experiments [7, 17, 22]. In further discussion the states obtained within the framework of the 8-band model will be labelled as ne_{m_f}, which represents the $n-$th electron state having the quantum number of the $z-$component of total angular momentum m_f (note that for each state ne_{m_f}, there is another state ne_{-m_f} with the same energy), and in a similar manner the state obtained by the effective mass method ne_m represents the $n-$th electron state having the quantum number of the $z-$component of orbital angular momentum m (note that for each state ne_m there also is an ne_{-m} state of the same energy). The dimensions of the embedding cylinder taken in all calculations are $R_t = 40\,\mathrm{nm}$, $H_t = 50\,\mathrm{nm}$, while the number of basis functions is determined from $n_{max} = 10$ and $l_{max} = 20$. It has been assumed in all calculations that a 0.5 nm wide wetting layer is present beneath each dot.

Since the choice of the embedding cylinder dimensions is arbitrary one has to check whether an increase in its dimensions leads to changes in the calculated spectrum. This is especially important when the transitions to continuum states dominate the spectral

response, as the continuum states are artificially discretized by embedding the quantum dot in a cylinder of finite size. Furthermore, it also has to be checked whether the number of basis functions taken in the calculation is sufficiently large. Such tests were performed by increasing each of the parameters R_t, H_t, n_{max} and l_{max}, while keeping the rest of them constant. No observable changes in the absorption spectra occurred during these tests.

It has also been checked that for all structures considered in this work the changes in absorption spectra with electric field are only slight and therefore the spectrum obtained at zero bias can be considered as representative of the spectrum for any value of the field. More specifically, in the range of fields typically used in QDIPs $-50\,\mathrm{kV/cm} < F < 50\,\mathrm{kV/cm}$, the positions of the absorption peaks change by less than 5% for all the structures considered (see figure 2 as an example). Clearly, these peaks cannot be observed in responsivity spectra at zero bias, but only when the bias is sufficient that the absorbed carriers can form photocurrent.

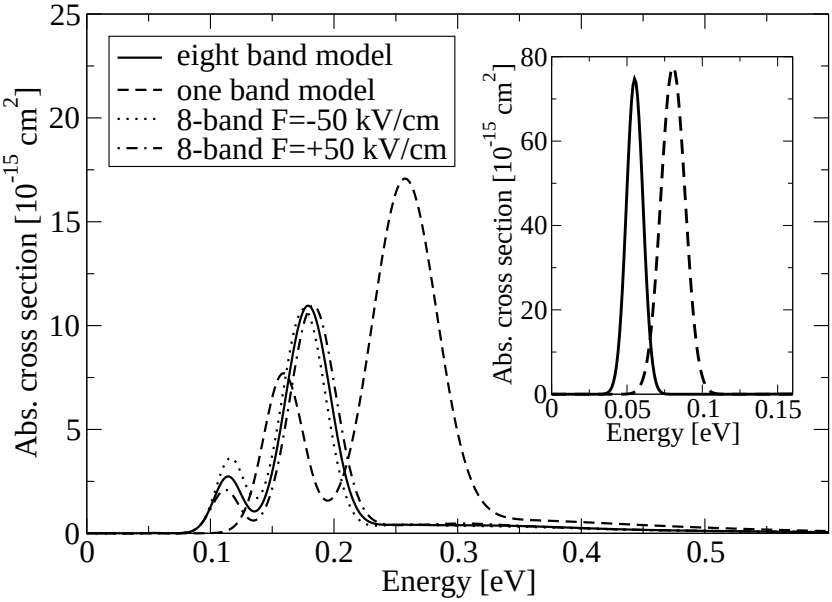

Figure 2. Intraband optical absorption spectrum for quantum dot of conical shape with the diameter $D = 25\,\mathrm{nm}$ and height $h = 7\,\mathrm{nm}$ in the case of $z-$polarized radiation. The corresponding spectrum for in-plane polarized radiation is shown in the inset. The absorption spectrum of $z-$polarized radiation calculated using the 8-band model at the fields of $F = -50\,\mathrm{kV/cm}$ and $F = 50\,\mathrm{kV/cm}$ is shown, as well.

We first compare the absorption spectrum obtained by the two methods for a quantum dot of conical shape with the diameter $D = 25\,\mathrm{nm}$ and height $h = 7\,\mathrm{nm}$, which are approximately the reported dimensions of quantum dots in a QDIP structure in [22] (the structure labelled as S-GaAs therein) based on the combination of atomic force microscopy and cross-sectional transmission electron microscopy measurements [22, 34].

The quantum dot is assumed to be of pure InAs as the growth conditions reported in [22] are such that intermixing between InAs and GaAs is minimized. The optical absorption spectrum in the case of $z-$polarized radiation is shown in figure 2. The two peaks in the spectrum originate from the transitions between bound states $1e_{1/2} \rightarrow 3e_{1/2}$ and $1e_{1/2} \rightarrow 5e_{1/2}$ ($k \cdot p$ model based labelling of states), i.e. $1e_0 \rightarrow 2e_0$ and $1e_0 \rightarrow 3e_0$ (effective mass model based labelling of states). The states $2e_{1/2}$ and $4e_{1/2}$ have opposite values of spin from $1e_{1/2}$ and transitions to them are therefore forbidden due to spin selection rules. The transitions to continuum states give a much smaller contribution to the spectrum. One can see from figure 2 that the results obtained by the two methods are qualitatively similar, however there are significant quantitative differences. The effective mass method gives larger values of transition energies and predicts stronger absorption. Since both the one and eight band method predict approximately the same position of the ground state with respect to the GaAs continuum (305 meV in one band vs. 295 meV in $k \cdot p$), one can ascribe these differences to non-parabolicity effects that are not properly taken into account within the simple effective mass approach. The one band model therefore underestimates the effective mass of the excited states which leads both to larger intersublevel energies and larger absorption matrix elements. The corresponding absorption spectrum for in-plane polarized incident radiation is presented in the inset of figure 2. There is a single peak in the spectrum which is due to the transition from the ground state $1e_{\pm 1/2}$ to a pair of nearly degenerate first excited states $2e_{\mp 1/2}$, $1e_{\pm 3/2}$. As in the case of $z-$polarized radiation, the peak position energy obtained by one band model is larger, which can be attributed to the same cause. The matrix elements of the dominant transition calculated within the effective mass method are larger. However, the difference between the transition energies (on the relative scale) is more prominent than in the case of $z-$polarized radiation, which therefore leads to only a slightly larger value of the peak absorption cross section within the effective mass model.

Next, the theoretical results obtained by the two methods are compared with the experimental results from [22] (figure 7a therein). One should have in mind that due to uncertainty in the determination of the dot size, as well as due to possible effects of In segregation and interdiffusion, any comparison between theoretical and experimental results should be taken with caution. The experimental intraband photocurrent spectrum exhibits the main peak at 175 meV and a much smaller peak at 115 meV, in excellent agreement with the results obtained for $z-$polarized incident radiation within the 8-band model where the corresponding peaks occur at 179 meV and 114 meV, respectively. It should be mentioned here that although the photocurrent spectrum in [22] is measured in the normal incidence geometry, the $z-$polarized component of incident radiation still exists due to the effects of off-normal axis experimental missalignment and extrinsic light scattering (For a nice discussion on this effect see for example [17,35], where the polarization dependent measurements in [17] have attributed the response measured in normal incidence geometry in [35] to $z-$polarized radiation, rather than in-plane polarized radiation). As already mentioned, the effective mass method gives peak positions at larger energies, which is only in qualitative agreement

with the experimental results.

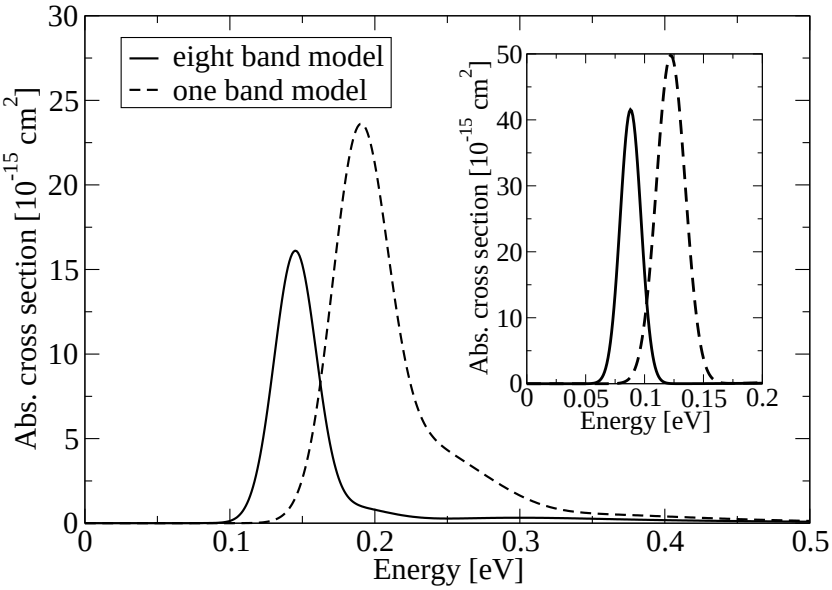

Figure 3. Intraband optical absorption spectrum for quantum dot in the shape of a truncated cone with the diameter of $D = 15\,\text{nm}$, height $h = 7\,\text{nm}$ and base angle of $\alpha = 60^0$, with $In_{0.15}Ga_{0.85}As$ layers of thickness $d = 6\,\text{nm}$ positioned both under and above the dot, surrounded by GaAs barriers, in the case of $z-$polarized radiation. The corresponding spectrum for the in-plane polarized radiation is shown in the inset.

We further analyze the intraband spectrum for the quantum dot in the shape of a truncated cone with the diameter of $D = 15\,\text{nm}$, height $h = 7\,\text{nm}$ and base angle of $\alpha = 60^0$ with $In_{0.15}Ga_{0.85}As$ layers of thickness $d = 6\,\text{nm}$ positioned both under and above the dot and surrounded by GaAs barriers. The dimensions were chosen to approximately match the dimensions of the quantum dots-in-a-well structure studied in [7] (the structure labelled as F therein). The optical absorption spectrum for $z-$polarized radiation is given in figure 3, while the inset shows the spectrum for the in-plane polarized radiation. In this case, there is a single peak for $z-$polarized radiation originating from $1e_{1/2} \rightarrow 3e_{1/2}$ ($1e_0 \rightarrow 2e_0$) transition ($2e_{1/2}$ has opposite value of spin to $1e_{1/2}$), while the same states as in the previous case are responsible for absorption of in-plane polarized radiation. Similarly to the previous structure considered, the effective mass approach predicts larger peak absorption energies and stronger absorption, which may be attributed to the same effect, as the positions of the ground state with respect to continuum calculated by the two methods are again almost the same (270 meV in eight band vs. 280 meV in one band model). The experimental results in [7] give the peak spectral response wavelength at 9.5 μm (figure 2 therein, curve labelled as F), the $k \cdot p$ method predicts the value of 8.6 μm, while the effective mass method gives 6.5 μm. The discrepancy between the results obtained by the $k \cdot p$ method and the experiment is

most likely due to the effects of intermixing of InAs and GaAs during growth at elevated temperatures.

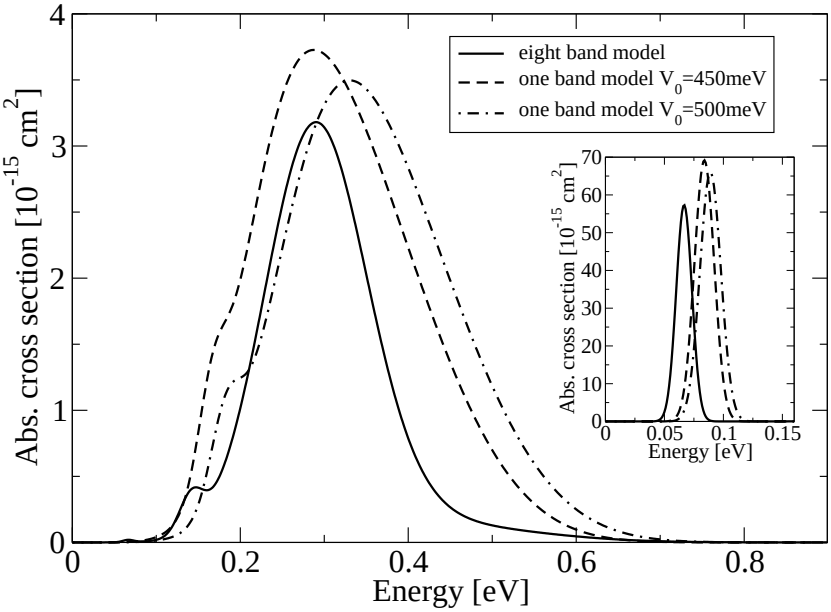

Figure 4. Intraband optical absorption spectrum for quantum dots in the shape of a lens with the diameter of $D = 20\,\text{nm}$, height $h = 3\,\text{nm}$ for $z-$polarized radiation. The corresponding spectrum for in-plane polarized radiation is shown in the inset.

Finally, we study a lens-shaped quantum dot, with a diameter $D = 20\,\text{nm}$ and a height $h = 3\,\text{nm}$. Quantum dots of similar shape and size were reported in several experiments [3, 14, 17, 35] and this is therefore one of the most typical shapes of InAs/GaAs self assembled quantum dots. The intraband optical absorption spectrum calculated by the two methods is shown in figure 4. The effective mass calculation was performed with two different values of the conduction band offset $V_0 = 450\,\text{meV}$ and $V_0 = 500\,\text{meV}$, because the calculated hydrostatic strain profile suggested that a larger value of V_0 than the conventional one (of 450 meV) should be used. Furthermore, the position of the ground state with respect to the onset of the GaAs continuum, calculated using the value $V_0 = 500\,\text{meV}$ is approximately the same as in the case of the $k \cdot p$ method (approximately 230 meV), in contrast to the smaller value of 190 meV when the conventional value of V_0 is used.

The dominant line in the absorption spectrum for in-plane polarized incident radiation stems again from the transition to a pair of (nearly) degenerate excited states. The position of the peak, at 66 meV, calculated within the $k \cdot p$ framework is within the range of experimentally observed values 55−85 meV [3, 17], while the effective mass method gives somewhat larger values. On the other hand, the main peak in the spectrum for $z-$polarized radiation originates from transitions to resonance states

in the continuum. In this case, the absorption spectrum calculated by the two methods gives almost the same peak position of 280 meV, when the same value of the conduction band offset is chosen as in the previous cases. The overestimation of intraband energies, due to the neglect of non-parabolicity effects, exists in the effective mass method in this case too, but it is compensated by the underestimation of the ground state position with respect to the continuum. When a larger value of the conduction band offset is taken, which puts the ground states at the same position, the peak calculated within the effective mass method appears at a larger energy. On the other hand, the experimental results in [3, 14, 17, 35] give the peaks in the range 150–300 meV.

While this work was focused on quantum dots whose shape exhibits cylindrical symmetry when the computational problem can be effectively reduced from three dimensional to two dimensional, we would like to briefly comment on the influence of the commonly reported truncated pyramidal shape on the results and conclusions of this work. It is not expected that for such a shape the overall conclusions in terms of identification of the dominant transitions for different polarizations of incident radiation and comparison of the two methods should change. To verify this, we have calculated the intraband absorption spectrum for an InAs/GaAs quantum dot in the shape of a truncated square-based pyramid with the base width of $b = 20\,\mathrm{nm}$, height $h = 5\,\mathrm{nm}$ and base angle of $\alpha = 60^0$, using the symmetry-based method described in [26] and [28]. The $k \cdot p$ method yields the absorption peak of in-plane polarized radiation originating from the transition from the ground state to a pair of nearly degenerate first excited states and the absorption peak of $z-$polarized radiation at 192 meV originating from the transition to one of the higher excited states having the same symmetry as the ground state. The effective mass method yields the corresponding peak at 289 meV. The results are therefore in agreement with our expectations. We have additionally performed calculations using the shape of a truncated cone of a similar size to the truncated pyramid and obtained peaks at similar energies, confirming the fact that there are no fundamental aspects of the findings that change when the shape is changed from a truncated cone to a truncated pyramid.

4. Conclusion

A simulation of several typical InAs/GaAs QDIP structures reported in the literature and a systematic comparison of the two methods used to calculate the intraband absorption is given. The results obtained by the two methods are in qualitative agreement – the transition from the ground state to the pair of first excited states is responsible for absorption of in-plane polarized radiation, while the absorption of $z-$polarized radiation is due to the transition to a higher excited bound state in the case of larger dots and due to the transition to resonance states in the continuum in the case of small and flat dots. On the other hand, quantitatively, the effective mass method overestimates both the transition energies and optical absorption cross sections. Therefore, while the simple and fast effective mass method can be quite useful

for general understanding of intraband absorption and assignment of the experimental peaks to different transitions, the $k \cdot p$ method is more appropriate for a study aiming to provide quantitative predictions.

Appendix

In order to calculate the Hamiltonian matrix elements, one needs to evaluate expressions of the form

$$U_i = \int_V b^*_{nml}(r,z,\varphi) T_i b_{n'm'l'}(r,z,\varphi)\, r\, \mathrm{d}r\, \mathrm{d}z\, \mathrm{d}\varphi.$$

The one-band Hamiltonian contains the terms of the form

$$\begin{aligned} T_1 &= F(r,z), \\ T_2 &= (k_x^2 + k_y^2)F(r,z), \\ T_3 &= k_z^2 F(r,z), \end{aligned}$$

and therefore after performing the integration one can see that the Hamiltonian matrix elements will only have terms of the form

$$\begin{aligned} U_1 &= \delta_{mm'} \int_0^{R_t} \mathrm{d}r\, r f_{nm} f_{n'm'} F_{l-l'}(r), \\ U_2 &= \delta_{mm'} \int_0^{R_t} \mathrm{d}r \left(r \frac{\mathrm{d}f_{nm}}{\mathrm{d}r} \frac{\mathrm{d}f_{n'm'}}{\mathrm{d}r} + mm' \frac{f_{nm} f_{n'm'}}{r} \right) F_{l-l'}(r), \\ U_3 &= \delta_{mm'} \int_0^{R_t} \mathrm{d}r\, r f_{nm} f_{n'm'} \left(\frac{2\pi}{H_t} \right)^2 ll' F_{l-l'}(r), \end{aligned}$$

where

$$F_{l-l'}(r) = \frac{1}{H_t} \int_{-H_t/2}^{H_t/2} \mathrm{d}z\, e^{-i\frac{2\pi}{H_t}(l-l')z} F(r,z).$$

The explicit form of the functions $F(r,z)$ is

$$F_a(r,z) = P_{\mathrm{QD}} \chi_{\mathrm{QD}}(\boldsymbol{r}) + P_{\mathrm{B}} \chi_{\mathrm{B}}(\boldsymbol{r}) + P_{\mathrm{QW}} \chi_{\mathrm{QW}}(\boldsymbol{r}),$$

and when the external bias is also included additional terms appear, which are of the form

$$F_b(r,z) = |e| F z.$$

P_{QD}, P_{B} and P_{M} are the values of the material parameter P in the dot, barrier and well respectively and χ_{QD}, χ_{B} and χ_{QW} are the functions equal to 1 inside and 0 outside the dot, barrier and quantum well (without the dot) region, respectively. The quantum well term clearly exist only in the case of quantum dots-in-a-well structures. The integral $F_{l-l'}(r)$ can then be performed analytically for each of quantum dot shapes with cylindrical symmetry. However, in the more general case when the indium composition varies smoothly (for example when the effects of segregation or intermixing occur), $F_a(r,z)$ is not piecewise constant, and the integration in $F_{l-l'}(r)$ has to be performed numerically. We have chosen this approach and performed numerical integration to keep

our simulation general enough such that the effects of a smooth variation of indium composition can be included as well.

In addition to the terms of type T_1, T_2, T_3, the elements of the kinetic part of the 8-band Hamiltonian contain the terms

$$\begin{aligned}
T_4 &= k_z F(r,z),\\
T_5 &= k_\mp F(r,z),\\
T_6 &= k_z k_\mp F(r,z),\\
T_7 &= k_\mp^2 F(r,z),
\end{aligned}$$

where $k_\pm = k_x \pm i k_y$. After the integration one finds that the corresponding terms in the Hamiltonian matrix are of the form

$$\begin{aligned}
U_4 &= \frac{\pi}{H_t}(l+l')U_1,\\
U_5 &= -\frac{i}{2}\delta_{m,m'\mp 1}\int_0^{R_t} \mathrm{d}r\, r F_{l-l'}(r) \times\\
&\times \left[f_{nm}\left(\frac{\mathrm{d}f_{n'm'}}{\mathrm{d}r} \pm m'\frac{f_{n'm'}}{r}\right) - f_{n'm'}\left(\frac{\mathrm{d}f_{nm}}{\mathrm{d}r} \mp m\frac{f_{nm}}{r}\right)\right],\\
U_6 &= -i\frac{\pi}{H_t}\delta_{m,m'\mp 1}\int_0^{R_t} \mathrm{d}r\, r F_{l-l'}(r) \times\\
&\times \left[l f_{nm}\left(\frac{\mathrm{d}f_{n'm'}}{\mathrm{d}r} \pm m'\frac{f_{n'm'}}{r}\right) - l' f_{n'm'}\left(\frac{\mathrm{d}f_{nm}}{\mathrm{d}r} \mp m\frac{f_{nm}}{r}\right)\right],\\
U_7 &= \delta_{m\pm 1,m'\mp 1}\int_0^{R_t} \mathrm{d}r\, r F_{l-l'}(r) \times\\
&\times \left(\frac{\mathrm{d}f_{nm}}{\mathrm{d}r} \mp m\frac{f_{nm}}{r}\right)\left(\frac{\mathrm{d}f_{n'm'}}{\mathrm{d}r} \pm m'\frac{f_{n'm'}}{r}\right).
\end{aligned}$$

The strain part of the Hamiltonian has terms of the type

$$\begin{aligned}
T_8 &= F(r,z)e_{ij},\\
T_9 &= F(r,z)e_{ij}k_\mp,\\
T_{10} &= F(r,z)e_{ij}k_z,
\end{aligned}$$

where e_{ij} are the strain tensor components. After performing the integration over φ, one gets

$$U_8 = \int_0^{R_t} \mathrm{d}r\, r f_{nm} f_{n'm'} \frac{1}{H_t}\int_{-H_t/2}^{H_t/2} \mathrm{d}z\, e^{-i\frac{2\pi}{H_t}(l-l')z}\overline{e}_{ij}(r,z),$$

where

$$\overline{e}_{ij}(r,z) = \frac{1}{2\pi}\int_0^{2\pi} \mathrm{d}\varphi\, e^{-i(m-m')\varphi} e_{ij}(r,z,\varphi),$$

and therefore the term U_8 becomes of the same form as U_1. In a similar manner, the terms U_9 and U_{10} are of the same form as U_5 and U_4.

References

[1] Pan D, Zeng Y P, Kong M Y, Wu J, Zhu Y Q, Zhang C H, Li J M and Wang C Y 1996 *Electron. Lett.* **32** 1726–1727

[2] Pan D, Towe E and Kennerly S 1998 *Appl. Phys. Lett.* **73** 1937–1939

[3] Maimon S, Finkman E, Bahir G, Schacham S E, Garcia J M and Petroff P M 1998 *Appl. Phys. Lett.* **73** 2003–2005

[4] Wang S Y, Lin S D, Wu H W and Lee C P 2001 *Appl. Phys. Lett.* **78** 1023–1025

[5] Stiff A D, Krishna S, Bhattacharya P and Kennerly S 2001 *Appl. Phys. Lett.* **79** 421–423

[6] Kim E T, Chen Z H and Madhukar A 2001 *Appl. Phys. Lett.* **79** 3341–3343

[7] Raghavan S, Forman D, Hill P, Weisse-Bernstein N R, von Winckel G, Rotella P, Krishna S, Kennerly S W and Little J W 2004 *J. Appl. Phys.* **96** 1036–1039

[8] Krishna S 2005 *J. Phys. D: Appl. Phys.* **38** 2142–2150

[9] Jiang J, Mi K, Tsao S, Zhang W, Lim H, O'Sullivan T, Sills T, Razeghi M, Brown G J and Tidrow M Z 2004 *Appl. Phys. Lett.* **84** 2232–2234

[10] Krishna S, Forman D, Annamalai S, Dowd P, Varangis P, Tumolillo T, Gray A, Zilko J, Sun K, Liu M G, Campbell J and Carothers D 2005 *Appl. Phys. Lett.* **86** 193501

[11] Bhattacharya P, Su X H, Chakrabarti S, Ariyawansa G and Perera A G U 2005 *Appl. Phys. Lett.* **86** 191106

[12] Fu L, Lever P, Sears K, Tan H H and Jagadish C 2005 *IEEE Electron Dev. Lett.* **26** 628–630

[13] Duboz J Y, Liu H C, Wasilewski Z R, Byloss M and Dudek R 2003 *J. Appl. Phys.* **93** 1320–1322

[14] Sauvage S, Boucaud P, Bruhnes T, Immer V, Finkman E and Gerard J M 2001 *Appl. Phys. Lett.* **78** 2327–2329

[15] Adawi A M, Zibik E A, Wilson L R, Lemaître A, Cockburn J W, Skolnick M S, Hopkinson M and Hill G 2003 *Appl. Phys. Lett.* **83** 602–604

[16] Zhang J Z and Galbraith I 2004 *Appl. Phys. Lett.* **84** 1934–1936

[17] Schrey F F, Rebohle L, Müller T, Strasser G, Unterrainer K, Nguyen D P, Regnault N, Ferreira R and Bastard G 2005 *Phys. Rev. B* **72** 155310

[18] Lim H, Zhang W, Tsao S, Sills T, Szafraniec J, Mi K, Movaghar B and Razeghi M 2005 *Phys. Rev. B* **72** 085332

[19] Han X, Li J, Wu J, Cong G, Liu X, Zhu Q and Wang Z 2005 *J. Appl. Phys.* **98** 053703

[20] Jiang X D, Li S S and Tidrow M Z 1999 *Physica E (Amsterdam)* **5** 27–35

[21] Stoleru V G and Towe E 2003 *Appl. Phys. Lett.* **83** 5026–5028

[22] Chen Z, Baklenov O, Kim E T, Mukhametzhanov I, Tie J, Madhukar A, Ye Z and Campbell J C 2001 *J. Appl. Phys.* **89** 4558–4563

[23] Amtout A, Raghavan S, Rotella P, von Winckel G, Stintz A and Krishna S 2004 *J. Appl. Phys.* **96** 3782–3786

[24] Cusack M A, Briddon P R and Jaros M 1996 *Phys. Rev. B* **54** R2300–R2303

[25] Grundmann M, Stier O and Bimberg D 1995 *Phys. Rev. B* **52** 11969–11981

[26] Vukmirović N, Indjin D, Jovanović V D, Ikonić Z and Harrison P 2005 *Phys. Rev. B* **72** 075356

[27] Ikonić Z, Milanović V and Tadić M 1995 *J. Phys.: Condens. Matter* **7** 7045–7052

[28] Vukmirović N, Ikonić Z, Jovanović V D, Indjin D and Harrison P 2005 *IEEE J. Quantum Electron.* **41** 1361–1368

[29] Bahder T B 1990 *Phys. Rev. B* **41** 11992–12001

[30] Tadić M, Peeters F M and Janssens K L 2002 *Phys. Rev. B* **65** 165333

[31] Jogai B 2000 *J. Appl. Phys.* **88** 5050–5055

[32] Press W H, Teukolsky S A, Vetterling W T and Flannery B P 1992 *Numerical recipes in Fortran 77* (Cambridge University Press, Cambridge)

[33] Vurgaftman I, Meyer J R and Ram-Mohan L R 2001 *J. Appl. Phys.* **89** 5815–5867

[34] Mukhametzhanov I, Chen Z H, Baklenov O, Kim E T and Madhukar A 2001 *Phys. Status Solidi B* **224** 697–702

[35] Rebohle L, Schrey F F, Hofer S, Strasser G and Unterrainer K 2002 *Appl. Phys. Lett.* **81** 2079–2081